7334 *Biochemistry* **2009,** *48,* 7334–7341
DOI: 10.1021/bi900467a

BIOCHEMISTRY
including biophysical chemistry & molecular biology
Article

The G18V CRYGS Mutation Associated with Human Cataracts Increases γS-Crystallin Sensitivity to Thermal and Chemical Stress

Zhiwei Ma,[‡] Grzegorz Piszczek,[§] Paul T. Wingfield,[∥] Yuri V. Sergeev,[‡] and J. Fielding Hejtmancik*[,‡]

[‡]*National Eye Institute and* [§]*National Heart, Lung, and Blood Institute and* [∥]*National Institute of Arthritis and Musculoskeletal and Skin Diseases, National Institutes of Health, Bethesda, Maryland 20892*

Received March 18, 2009; Revised Manuscript Received June 8, 2009

ABSTRACT: γS-Crystallin, important in maintaining lens transparency, is a monomeric βγ-crystallin comprising two paired homologous domains, each with two Greek key motifs. An autosomal dominant cortical progressive cataract has been associated with a G18V mutation in human γS-crystallin. To investigate the molecular mechanism of this cataract and confirm the causative nature of the G18V mutation, we examined resultant changes in conformation and stability. Human γS-crystallin cDNA was cloned into pET-20b(+), and the G18V mutant was generated by site-directed mutagenesis. Recombinant HγS-crystallins were expressed in *Escherichia coli* and purified by ion-exchange and size-exclusion chromatography. By analytical ultracentrifugation wild-type and mutant HγS-crystallins are monomers of about 21.95 ± 0.21 and 20.89 ± 0.18 kDa, respectively, and have similar secondary structures by far-UV CD. In increasing levels of guanidine hydrochloride (GuHCl), a sharp red shift in fluorescence λ_{max} and increase in emission correlating with exposure of tryptophans to the protein surface are detected earlier in the mutant protein. Under thermal stress, the G18V mutant begins to show changes in tryptophan fluorescence above 42 °C and shows a T_m of 65 °C as monitored by CD at 218 nm, while wild-type HγS-crystallin is very stable with T_m values of 75.5 and 75.0 °C as measured by fluorescence and CD, respectively. Equilibrium unfolding/refolding experiments as a function of GuHCl confirm the relative instability of the G18V mutant. Wild-type HγS-crystallin exhibits a two-state transition and reversible refolding above 1.0 M GuHCl, but the unfolding transition of mutant HγS-crystallin shows an intermediate state. The first transition (N → I) shows a $[GuHCl]_{1/2}$ of 0.5 M while the second transition (I → U) has the same $[GuHCl]_{1/2}$ as wild-type HγS-crystallin, about 2.0 M. Our present study confirms the high stability of wild-type HγS-crystallin and demonstrates that the G18V mutation destabilizes the protein toward heat and GuHCl-induced unfolding. These biophysical characteristics are consistent with the progressive cataract formation seen in the family members carrying this mutation.

The lens is an avascular cellular ocular tissue with a high refractive index and a high degree of transparency. These properties are the result of high concentrations of structural proteins called lens crystallins. In the fully formed lens, there is a single layer of epithelial cells inside the anterior capsule, which divide and migrate to the equator, where they elongate to form fiber cells. Terminally differentiated fiber cells in the lens are anucleate and devoid of all other organelles and are unable to degrade damaged crystallins or to synthesize new ones. Therefore, crystallins must be stable throughout the lifespan of the organism despite high concentrations of protein, continual UV exposure, and potential oxidative stress.

Three major classes of ubiquitous crystallins (α, β, and γ) are the predominant structural proteins in the eye lens throughout all vertebrates. β- and γ-crystallins are evolutionarily and structurally related and constitute the βγ-crystallin superfamily (*1*). They have close to 30% sequence identity and similar polypeptide chain folds including a two-domain structure with each domain comprising two intercalated antiparallel β-sheet Greek key motifs. Each Greek key motif has a glycine residue at the apex, as the torsional angles required at this position are denied to or strained for amino acids with side chains (*2*). The γ-crystallins seem to be particularly adapted for the highest concentrations in the central regions of the lens. Gene and structural alignment comparisons suggest that β- and γ-crystallins evolved from a common ancestral protein (*3*). γ-Crystallins are more stable than the α- and β-crystallins, with γS-crystallin probably less stable than the other branch of γ-crystallins given the conditions required for denaturation of the γA-F-crystallins (*4*). γS-Crystallin is highly conserved in evolution (*5*) and is expressed late but abundantly in the cortical regions of the lens and even in epithelial cells (*6*). A G18V point mutation in γS-crystallin has previously been identified in affected members of a Chinese family, leading to progressive cortical cataracts (*7*).

It has been suggested that crystallin mutations sufficient by themselves to cause protein aggregation are seen in congenital cataracts with a Mendelian inheritance pattern, while sequence changes that merely increase susceptibility to environmental insults might contribute to age-related cataracts, which tend to show complex inheritance (*8*). Both seem likely to result in crystallin misfolding and unfolding and/or in altered interactions and association among native, modified, and defective crystallins leading to poorly soluble high-molecular-mass aggregates (*4*). The progressive cortical cataracts in this family show Mendelian inheritance with complete penetrance, suggesting that it might also have an intermediate effect on crystallin structure compared

*Address correspondence to this author at MOGS/OGVFB/NEI/NIH, Room 1120, 5635 Fisher's Lane, Rockville, MD 20852. Tel: 301-496-8300. Fax: 301-435-1598. E-mail: f3h@nei.nih.gov.

 Published on Web 06/26/2009

to most genetic contributions to congenital and age-related cataracts. The focus of this study is to investigate the molecular effect of the G18V mutation on HγS-crystallin[1] by comparing the conformation and stability of the mutant with the wild-type γS-crystallin under both normal and stressed conditions. The G18V mutant γ-crystallin has a normal structure under mild conditions but is more susceptible to denaturation under both thermal and chemical stress. This behavior is consistent with and in part explains the inheritance pattern and phenotype seen in affected members of the family with this mutation.

MATERIALS AND METHODS

Cloning and Site-Directed Mutagenesis. The cDNA coding for human γS-crystallin was amplified from a human lens cDNA library using PCR primers containing *Nde*I and *Xho*I sites (F, cggcatatgtctaaaactggaacc; R, cggctcgagttactccacaatgc) and was cloned into the plasmid pCR2.1 (Invitrogen). The cloned DNA was verified by DNA sequencing and then digested using *Nde*I and *Xho*I restriction endonucleases (New England Biolabs). The fragment was subcloned into the pET-20b(+) vector (Novagen) between the *Nde*I and *Xho*I sites. Site-directed mutagenesis was performed using two complementary primers (F, gacaaaaattttcaagtccgtcgctatgactgtg; R, cacagtcatagcgacggacttgaaaatttttgtc) including the desired mutation and template vector pET-20b(+)-γS. The wild-type and mutant constructs were sequenced to confirm the substitution and the absence of nonspecific mutations.

Protein Expression and Purification. Wild-type and mutant HγS-crystallins were expressed in BL21(DE3) cells. The *Escherichia coli* cells were grown in LB broth to $OD_{600} = 1$ at 37 °C with shaking of 250 rpm and then induced with 0.5 mM isopropyl β-D-thiogalactopyranoside (IPTG). After incubation for another 2 h at 37 °C (wild type) and 27 °C (mutant), the cells were harvested and frozen at −80 °C until use.

Wild-type and mutant HγS-crystallins were purified using the same method. Briefly, cells were sonicated on ice in buffer: 50 mM Tris-HCl, pH 7.5, 1 mM EDTA, 1 mM dithiothreitol (DTT), 50 μM tris(2-carboxyethyl)phosphine (TCEP), and 2.8 mM Mini-complete protease inhibitor (Roche). All lysates were centrifuged at 14000 rpm for 30 min at 4 °C, and the supernatants were dialyzed in a 10000 MWCO dialysis cassette (Pierce) overnight against 2 L of buffer A: 50 mM sodium acetate, 1 mM EDTA, 1 mM DTT, and 50 μM TCEP, pH 5.4. Soluble extracts were purified at room temperature using a FPLC Bio-Logic Duo-Flow workstation (Bio-Rad, Hercules, CA). Proteins were first purified by ion-exchange chromatography using a 5 mL Hi-Trap SP column equilibrated with buffer A. Proteins were loaded on the column at a flow rate of 0.5 mL/min, a 0.1 M NaCl salt gradient was applied, and 2.5 mL fractions were collected. To obtain γS-crystallin with >95% purity, it was necessary to perform further purification by size-exclusion chromatography using a 1.6 cm × 60 cm (124 mL) Superdex-75 HR column (Amersham Biosciences) equilibrated in buffer B: 50 mM Tris-HCl, pH 7.5, 1 mM EDTA, 1 mM DTT, 0.15 M NaCl, and 50 μM TCEP. The flow rate was 0.5 mL/min, and 0.5 mL fractions were collected. The column was precalibrated with five standards: thyroglobulin, γ-globulin, ovalbumin, myoglobin, and vitamin B_{12} (Bio-Rad). The location of recombinant proteins in column fractions was monitored by absorbance at 280 nm and by SDS−PAGE using 12% polyacrylamide gels. Protein identity was confirmed by Western blot analysis.

Analytical Ultracentrifugation. Only samples showing a single peak on analytical gel filtration columns and which were greater than 95% pure as judged by SDS−PAGE were used for analytical ultracentrifugation. To minimize artifactual association of proteins due to sulfhydryl oxidation, samples (10 μM) were incubated for 1 h at room temperature in buffer C containing 10 mM DTT and 1.5 M urea, followed by dialysis for 24 h at 4 °C against 1 L of buffer C. Prior to a centrifugation, 50 μM reductant tris(2-carboxyethyl)phosphine (TCEP; Pierce Biotechnology Inc., Rockford, IL) was added to the proteins and reference buffer. Centrifugation was carried out using a Beckman Optima XL-I analytical ultracentrifuge (*9*). Absorption optics, an An-60 Ti rotor, and standard double-sector centerpiece cells were used. All analyses were performed using duplicate protein samples. Data were collected after 16−20 h (20 °C) at 21500 rpm. Equilibria profiles were analyzed using standard Optima XL-I Origin based data analysis software.

CD spectroscopy. Far- and near-UV CD measurements were performed on a Jasco-715 (Jasco Inc., Tokyo, Japan) spectropolarimeter at room temperature. Far-UV CD spectra were recorded between 185 and 250 nm using a 0.02 cm path length. For near-UV CD studies, a 1 cm path length was used, and the spectra were recorded between 250 and 350 nm. Protein samples were prepared in buffer containing 10 mM sodium phosphate (pH 7.0) and 50 μM TCEP. All measurements were corrected by background subtraction, and each spectrum presented is the average of at least 10 scans. Data was analyzed to determine secondary structure percentage using the CDPro program (*10*, *11*).

Fluorescence Spectroscopy. Intrinsic tryptophan fluorescence was measured using Cary Eclipse fluorescence spectrophotometer (Varian). An excitation wavelength of 280 nm was applied, whereas emission spectra were recorded in the range between 300 and 400 nm. All fluorescence spectra were corrected for the buffer baseline.

ANS Binding. The binding of the hydrophobic probe 8-anilino-1-naphthalenesulfonate (ANS) to wild-type and G18V mutant HγS-crystallins was assessed by recording fluorescence spectra with excitation at 370 nm and emission between 400 and 600 nm. Before testing, protein (1 μM) and ANS (50 μM) were incubated in PBS for 30 min at 25 °C.

Thermodynamic Analysis. Thermostability of the normal and G18V mutant γS-crystallins was monitored by recording the fluorescence emission at 328 and 355 nm with a programmable temperature controller at a scan rate of 1.0 °C/min. Thermostability was confirmed by measuring the circular dichroism spectra at 218 nm using a 0.05 cm path length. Protein samples were prepared in buffer containing 10 mM sodium phosphate (pH 7.0), 0.15 M NaCl, and 50 μM TCEP. Denaturation curves were analyzed using Graphpad Prism 5 software according to the method of Pace (*12*). The ΔG values were plotted as a function of temperature to determine T_m and ΔH_m. The enthalpy change ΔH was calculated using the van't Hoff equation: $d(\ln K)/d(1/T) = -\Delta H/R$.

Equilibrium Unfolding/Refolding. Equilibrium unfolding experiments were carried out by diluting purified wild-type and mutant proteins to 1 μM in increasing concentrations of GuHCl from 0 to 6 M. Buffer conditions for all unfolding samples were 50 mM Tris-HCl, 1 mM EDTA, 5 mM DTT, 0.15 M NaCl, and 50 μM TCEP. The unfolding samples were incubated at room

[1]Abbreviation: HγS-crystallin, human γS-crystallin.

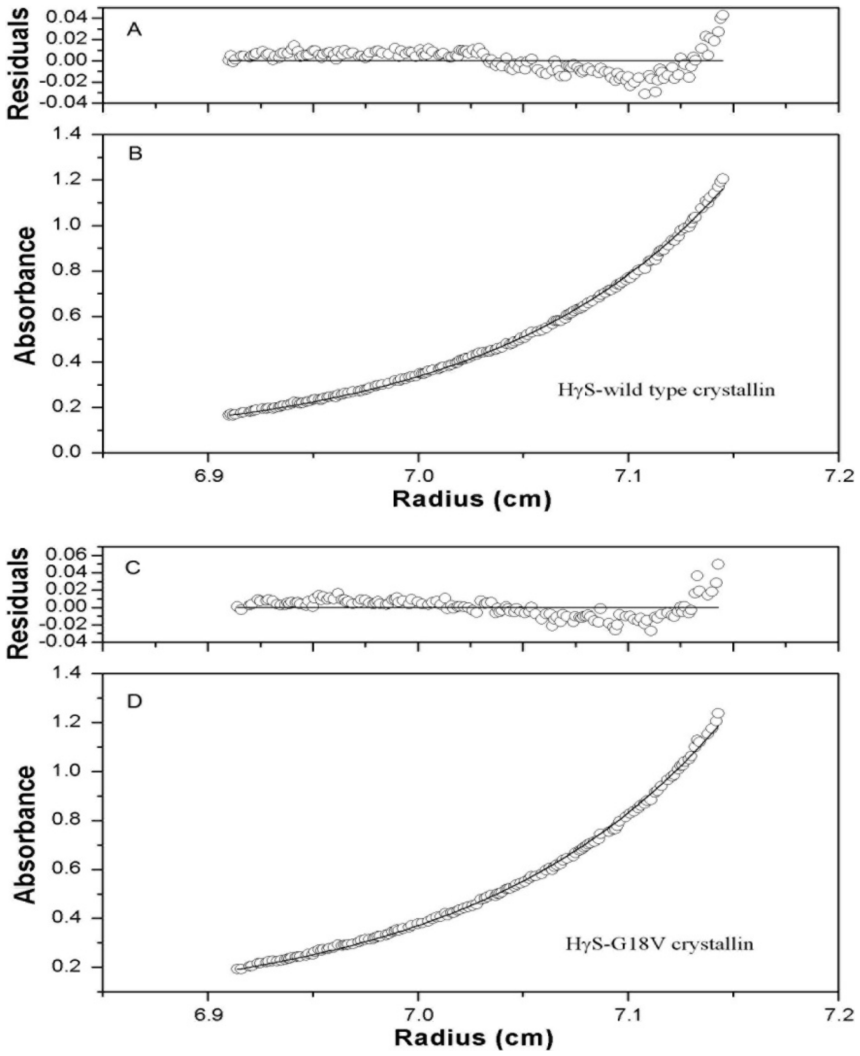

FIGURE 1: Sedimentation equilibrium data obtained for wild-type and mutant HγS-crystallins at 20 °C. Absorbance (B, D) and residuals (A, C) ploted for wild-type and mutant HγS-crystallins. Open circles show the protein concentration profile represented by the UV absorbance gradients in the centrifuge cell at 280 nm. The solid lines indicate the calculated fit for the monomer.

temperature for 24 h, by which time equilibrium had been reached.

Equilibrium refolding experiments were carried out by initially preparing an unfolded stock solution containing 60 μM purified protein in 6 M GuHCl. The unfolded stock solution was incubated at 37 °C for 6 h and then diluted into refolding buffer to a final protein concentration of 1 μM. Refolding buffer contained 50 mM Tris-HCl, pH 7.5, 1 mM EDTA, 5 mM DTT, 0.15 M NaCl, and 50 μM TCEP and GuHCl from 0.1 to 6 M. The refolding samples were allowed to reach equilibrium by incubation at room temperature for 24 h. Fluorescence emission spectra were recorded for all unfolding/refolding samples by using an excitation wavelength of 280 nm and monitoring emission from 300 to 400 nm. Unfolding/refolding transitions were analyzed in terms of wavelength shifts of the emission peak and by calculating the peak ratios of intensities as measured at 328 and 355 nm (FI 355/328 nm). The ratio of fluorescence intensities at these wavelengths was chosen for the analysis in order to simultaneously monitor changes in the native and unfolded maxima. Equilibrium unfolding/refolding experiments were performed a minimum of four times for each protein. Equilibrium unfolding/refolding data were analyzed using Graphpad Prism 5 software; ΔG° and m values were calculated using the method of Pace (*13*).

RESULTS

Protein Purification and Characterization. After the presence of the desired substitution and the absence of nonspecific changes in the constructs were confirmed, the wild-type and mutant HγS-crystallins were expressed and purified to high (> 95%) purity as judged by SDS−PAGE using cation-exchange chromatography and gel filtration chromatography.

Sedimentation equilibrium centrifugation at 20 °C shows the native molecular masses of wild-type and mutant HγS-crystallins to be 21.95 ± 0.21 and 20.89 ± 0.18 kDa, respectively. The apparent molecular masses are consistent with the predicted monomer masses, and a monomer model is most consistent with the sedimentation curves and was applied to the analyses of the equilibrium profiles (Figure 1B,D). The residuals from the model scatter randomly around zero, although there is a slight systematic trend for errors of both wild-type and mutant HγS-crystallins near the bottom (Figure1A,C). This is most likely due to the presence of small amounts (< 5%) of higher order irreversible aggregates.

No gross differences in the secondary structure of the wild type and G18V mutant are seen on CD. Under nondenaturing conditions, the far-UV CD of wild-type HγS-crystallin displays a strong minimum at 218 nm, consistent with a high β-sheet content, in accord with previous reports (*14*). The G18V mutant

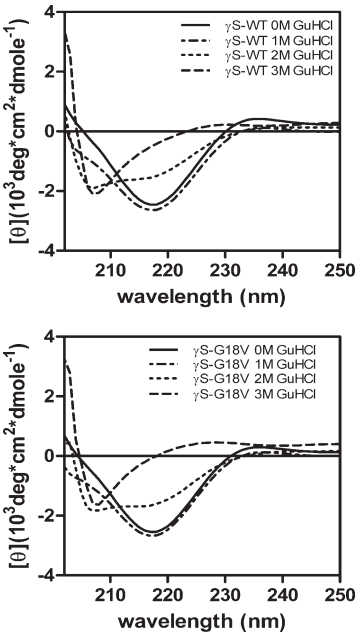

FIGURE 2: Far-UV CD spectra of wild-type (top) and G19V mutant (bottom) γS-crystallin in increasing concentrations of GuHCl.

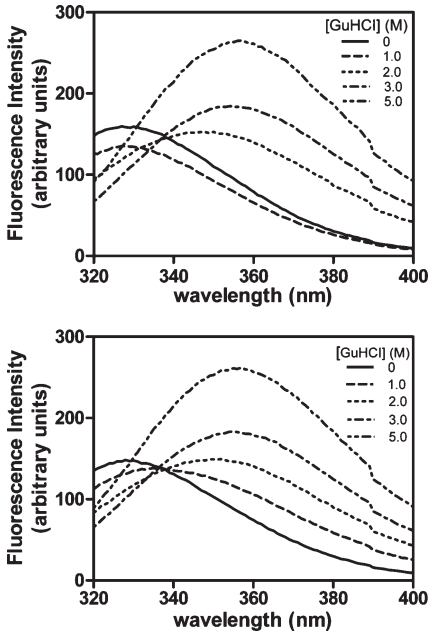

FIGURE 3: Fluorescence emission spectra of wild-type (top) and G18V mutant (bottom) γS-crystallin in increasing concentrations of GuHCl.

Table 1: Deconvoluted CD Spectra and Fluorescence Emission Spectra Maxima for Wild-Type and Mutant HS-Crystallin

protein	% helix	% β-sheet	% turn	% unordered	λ_{max} fluorescence emission (nm)
WT 0 M GuHCl	1.7	42.03	21.25	33.88	328
MUT 0 M GuHCl	2.03	41.28	21.93	33.78	328
WT 1 M GuHCl	2.38	40.95	22.83	32.73	328
MUT 1 M GuHCl	2.2	40.48	22.05	34.25	336
WT 2 M GuHCl	4.35	40.78	20.93	33.13	347
MUT 2 M GuHCl	3.27	39.8	21.88	35.55	350
WT 3 M GuHCl	12.5	37.27	18.28	29.08	355
MUT 3 M GuHCl	8.93	35.57	21.95	30.3	355

has a spectrum similar to that of the wild type (Figure 2). Upon denaturation, the far-UV signals of both the wild type and G18V mutant show a large change due to loss of secondary structure, but no differences are seen in the far-UV signals between the wild-type and mutant proteins in the same concentration of GuHCl. These CD spectra were further analyzed using the deconvolution software, CDPro Suite, to determine quantitative percentages of secondary structure. Deconvolution of the CD spectra agreed with qualitative observations that the WT and mutant β-sheet structures were indistinguishable (Table 1). The near-UV CD spectra of wild-type HγS-crystallin and mutant proteins superimpose (data not shown).

Protein Denaturation. HγS-Crystallin contains four buried tryptophan (Trp) residues. Each of the two domains contains two buried Trp residues in its hydrophobic core, allowing these four Trp chromophores to be used as probes to monitor changes in the tertiary structures of the proteins. The spectral changes associated with the denaturation of wild-type and mutant HγS-crystallins were studied by circular dichroism and fluorescence spectroscopy in different concentrations of GuHCl. In addition, thermal denaturation was used to assess the stability qualitatively.

As shown in Figure 3, native wild-type HγS-crystallin has a fluorescence maximum at about 328 nm that increases in intensity

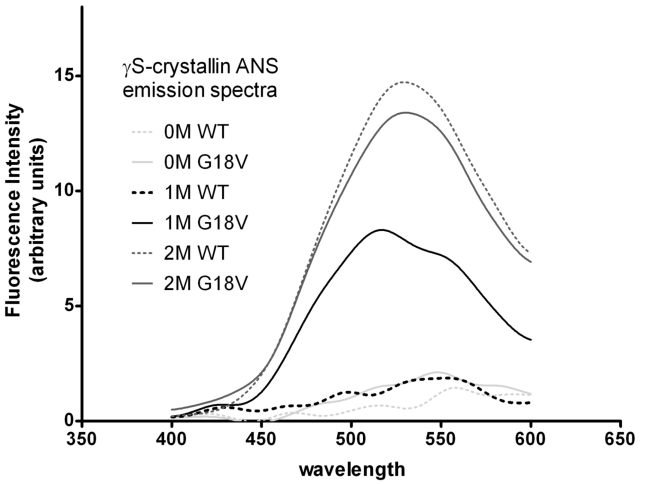

FIGURE 4: ANS emission spectra of wild-type and G18V HγS-crystallin in the presence of 0, 1, and 2 M GuHCl.

and shifts to approximately 355 nm upon treatment with 5 M GuHCl. Tryptophan emission of the G18V mutant was measured in a fashion analogous to that of the wild-type HγS-crystallin. Under native conditions the mutant protein exhibits an emission maximum of 328 nm, similar to that of the wild type. The GuHCl-denatured mutant protein has a maximum fluorescence emission at 355 nm, also similar to the wild type (Figure 3). Thus, under denaturing conditions, both proteins exhibit increased fluorescence intensity and a red shift in λ_{max}. However, significant differences between wild-type and mutant proteins occur at intermediate levels of GuHCl. In 1 M GuHCl solution, the fluorescence maximum of the G18V mutant HγS-crystallin is red shifted compare to the native state, while that of the wild type has no shift. ANS binding further confirms that hydrophobic area regions in the mutant protein are exposed to the protein surface under less denaturing conditions than the wild type (Figure 4). These results suggest that the G18V mutation does not disrupt the structure of HγS-crystallin in its native state, but it makes the

protein less stable to denaturing conditions. This difference in stability between the wild type and G18V mutant was further investigated through monitoring the sensitivity of the proteins to thermal denaturation.

The sensitivity of the two proteins to thermal denaturation was estimated by monitoring the FI ratio as well as circular dichroism at 218 nm. To provide the best analysis of the transition, the ratio of fluorescence intensities at 355 and 328 nm (FI355/328 nm) was plotted as a function of temperature (Figure 5A). The FI ratio of the wild-type HγS-crystallin sample does not alter significantly until 69 °C, at which point it increases sharply in a single transition, with no further denaturation above this temperature. In contrast, the G18V mutant HγS-crystallin sample exhibits an increasing FI ratio beginning at 42 °C. Upon further heating, a gradual transition is seen between 42 and 65 °C, and above 65 °C a sharp increase occurs. Analysis of these curves is consistent with the wild-type HγS-crystallin being extremely stable with a single T_m value of 75.5 °C. The G18V mutant protein is less stable compared to the wild type. It shows two transitions, with the first T_m at 61.49 and the second at 69.45 (Table 2). The change in ΔG with temperature for each transition is shown in Figure 6A, and the corresponding plots for the van't Hoff equation are shown in Figure 6B. The corresponding values of ΔH, ΔS, and $\Delta(\Delta G)$ are shown in Table 2.

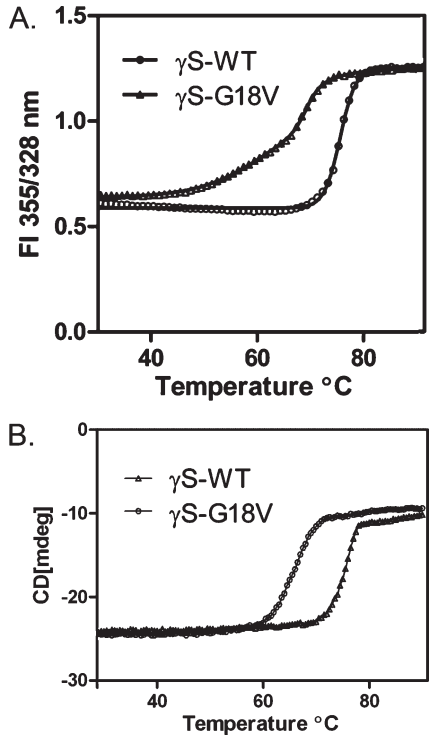

FIGURE 5: Thermal denaturation curves of wild-type and G18V mutant HγS-crystallins. (A) Tryptophan fluorescence. (B) CD at 218 nm.

In contrast to the denaturation curve obtained with tryptophan fluorescence, when the circular dichroism at 218 nm is monitored with increasing temperature, a single transition is observed for both the wild-type and G18V mutant HγS-crystallins (Figure 5B). Once more, the wild-type HγS-crystallin does not alter significantly until approximately 70 °C, at which point it rises in a sharp single transition complete by 79 °C. The G18V mutant also shows a single transition, although it is shifted to approximately 65 °C, beginning at 60 °C and finishing by 70 °C. The changes in ΔG with temperature for each transition are shown in Figure 6C, and the corresponding plots for the van't Hoff equation are shown in Figure 6D. These are in good agreement with the values obtained from tryptophan fluorescence, except for the absence of the early transition I in the CD data.

Equilibrium Unfolding and Refolding of Wild-Type and Mutant HγS-Crystallin. Equilibrium unfolding/refolding experiments were performed by monitoring intrinsic fluorescence emission. The ratio of fluorescence intensities at 355 and 328 nm (FI 355/328 nm) was plotted as a function of GuHCl concentration (Figure 7). The equilibrium unfolding transition of wild-type HγS-crystallin was fitted to a two-state model, yielding a midpoint of 1.96 M GuHCl for the native to unfolded transition. In contrast, the equilibrium unfolding/refolding transitions of the G18V mutant differ significantly from those of the wild type. A plateau extending from ~0.8 to ~1.8 M GuHCl is present in the unfolding and refolding transition as monitored by both peak wavelength and FI 355/328 nm, consistent with the presence of a partially folded intermediate. The equilibrium unfolding transition best fits a biphasic model with transition midpoints of 0.5 and 2.0 M GuHCl for the first and second transitions, respectively (Table 3).

Although a native-like conformation was attained when the proteins were refolded to 1.0−1.4 M GuHCl, continued refolding of wild-type HγS-crystallin to GuHCl concentrations below 1.0 M resulted in protein aggregation. This was seen as a sharp increase in FI 355/328 nm due to right-angle light scattering by the aggregate (*15*). On refolding the G18V mutant could not attain a native-like conformation, and subsequently the mutant protein aggregates more readily than the wild type (Figure 7).

DISCUSSION

Here we have examined the molecular effect of the G18V mutation on HγS-crystallin by comparing the conformation and stability of the mutant with the wild-type γS-crystallin under both normal and stressed conditions. G18, along with the adjacent two amino acids F16 and Q17, is conserved in all $\beta\gamma$-crystallins in all species from zebra fish to humans. One reason for this is that

Table 2: Thermal Denaturation Parameters of Wild-Type and Mutant HγS-Crystallin

protein	ΔS_m[a]	ΔH_m (kcal/mol)[b]	T_m[c]	ΔT_m[d]	$\Delta(\Delta G)$[e]
WT (FI ratio curve)	0.462 ± 0.014	161.057 ± 4.940	75.56 ± 0.15		
MUT (FI ratio curve) N ↔ I	0.099 ± 0.001	33.231 ± 0.379	61.49 ± 0.17	−14.07	−6.498
MUT (FI ratio curve) I ↔ U	0.318 ± 0.012	108.963 ± 4.064	69.45 ± 0.25	−6.11	−2.822
WT (CD curve)	0.440 ± 0.018	153.2 ± 6.269	75.05 ± 0.16		
MUT(CD curve)	0.219 ± 0.036	74.2 ± 12.192	65.46 ± 0.15	−9.59	−4.219

[a] Slope of ΔG versus T at T_m in kcal mol^{-1} deg^{-1}. [b] $\Delta H_m = [T_m(K)](\Delta S_m)$ in kcal/mol. [c] Midpoint of thermal unfolding curve in °C. [d] Difference between the T_m values. [e] $\Delta(\Delta G) = \Delta T_m \Delta S_m$, where ΔS_m is the value for the wild-type protein.

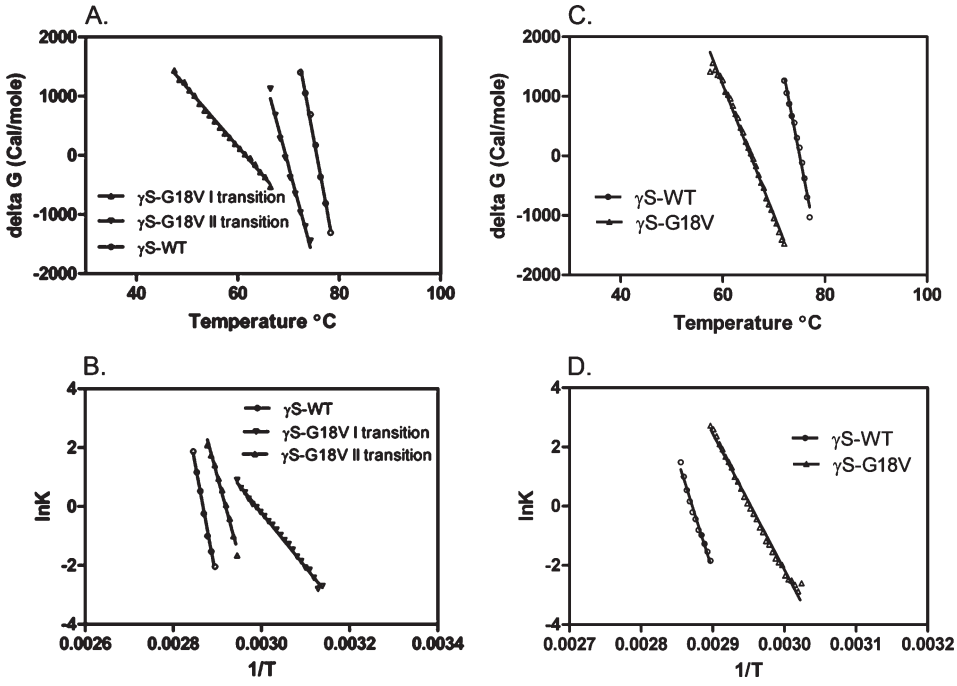

FIGURE 6: Plots of the ΔG values of wild-type and G18V mutant γS-crystallin as a function of temperature and calculation of the van't Hoff equation: $d(\ln K)/d(1/T) = -\Delta H/R$. (A) ΔG plot from tryptophan fluorescence in Figure 5A. (B) van't Hoff plot from tryptophan fluorescence in Figure 5A. (C) ΔG plot from CD at 218 nm in Figure 5B. (D) van't Hoff plot from CD at 218 nm in Figure 5B.

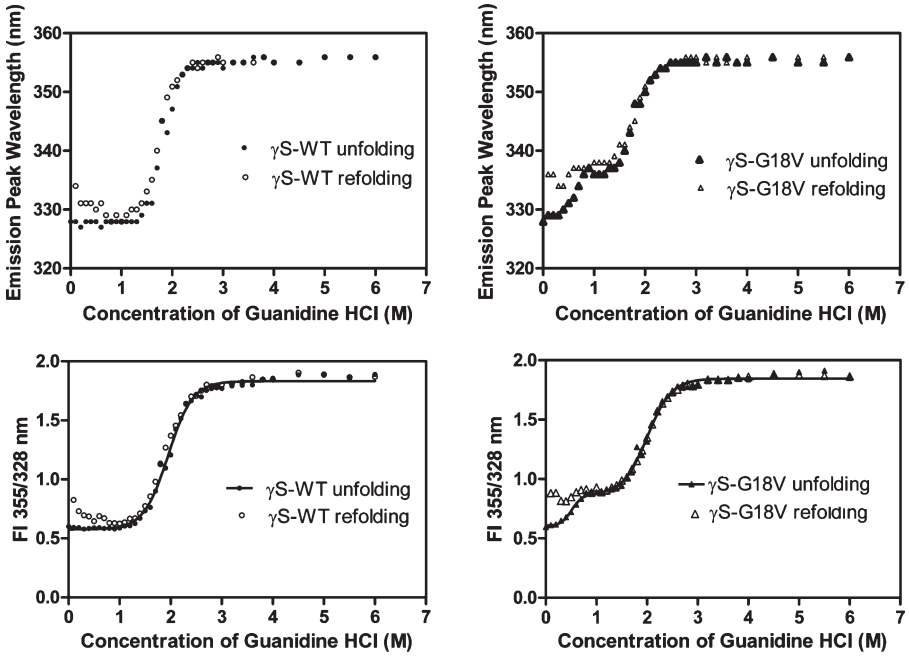

FIGURE 7: GuHCl-induced equilibrium unfolding/refolding of wild-type and mutant HγS-crystallin.

Table 3: Equilibrium Unfolding/Refolding at 25 °C Parameters of Wild-Type and Mutant HγS-Crystallin

protein	$\Delta G°$ (kcal/mol)[a]	m (kcal mol^{-1} M^{-1})	$[GuHCl]_{1/2}$
WT	4.832 ± 0.234	2.464 ± 0.115	1.961 ± 0.039
MUT N ↔ I	2.583 ± 0.180	5.141 ± 0.346	0.503 ± 0.031
MUT I ↔ U	5.234 ± 0.275	2.605 ± 0.136	2.009 ± 0.037

[a] Free energy of unfolding in the absence of GuHCl.

glycine, which lacks a side chain, is the only amino acid able to achieve the dihedral angle required to stabilize the folded hairpin of the $\beta\gamma$ motif (*16*). The presence of a residue with a side chain would be expected to expand and to some extent destabilize the Greek key structure of the first motif, but not necessarily to alter the association or solubility of the γS-crystallin protein. However, examination of the normal and G18V mutant under mild conditions shows little difference. The secondary structure of the G18V mutant protein, judged by CD spectra, indicates it has a native-like conformation similar to that of wild-type HγS-crystallin, and its association properties are identical to those of normal γS-crystallin. The native state fluorescence emission maximum of 328 nm and an unfolded maximum of 355 nm displayed in this study by wild-type and mutant HγS-crystallin are similar to those previously reported (*14*, *17*). Analytical

sedimentation equilibrium demonstrates that the wild-type and mutant HγS-crystallins are monomeric species in their native states, once more in agreement with previous findings (*14*, *17*, *18*). The fluorescence emission intensity increased upon unfolding, indicating that the tryptophans were quenched in the native fold. This phenomenon has been described previously for several of the γ-crystallins (*15*, *19*) and is proposed to relate to charge transfers from the buried tryptophans to the backbone of the polypeptide chain.

While the structure of the G18V mutant HγS-crystallin under mild conditions appears to be similar to that of the wild type, there is strong evidence that the G18V mutation decreases the stability of HγS-crystallin. Although the CD spectra of the native and G18V mutant in aqueous buffer are indistinguishable and similar to previously reported results (*14*), as are the spectra under completely denaturing conditions, in 1 M GuHCl the fluorescence emission maximum of the G18V mutant but not the wild type is red shifted. This suggests that the microenvironment of aromatic amino acids was altered and is consistent with partial denaturation of the G18V mutant. This is similar to the fluorescence emission spectra of the wild-type and G18V mutant proteins under increasing concentrations of GuHCl. Decreased stability of the mutant relative to the wild type is further supported by the ANS binding results. ANS is an anionic fluorescence probe that binds to the apolar interface and exhibits a shift in the emission maxima due to changes in hydrophobic patches on protein misfolding. In the conventional model aggregation is dominated by hydrophobic interactions of side chains that are normally buried in the native state but that are more exposed in an unfolded, non-native state (*20*). Thus, sensitivity to aggregation can derive from the ability of a mutation either to facilitate the accumulation of a non-native state that is prone to aggregation or to increase the intrinsic tendency of the mutant protein to aggregate.

The thermodynamic studies provide additional information about the effects of the G18V mutation on stability. The fluorescence emission spectra at 328 and 355 nm were recorded, and their ratio was used to estimate the molar fractions of folded and unfolded protein in aqueous solutions as a function of temperature, allowing quantitative estimation of the stability of the wild-type and mutant proteins (*21*). It has previously been shown that the N-terminal domain of γS-crystallin ($\gamma S_N T_m$ = 69.1 °C) is less stable than the C-terminal domain ($\gamma S_C T_m$ = 75.1 °C), and the T_m of γS_C was similar to the T_m of the full-length γS (*14*). However, when the intact γS-crystallin was examined, a two-state model was found to be sufficient to fit the experimental data (*17*) even though there are suggestions of more complex behavior, and we confirmed this as well ($H\gamma S_{wt} T_m$ = 75.6 °C).

The G18V mutation dramatically decreases the thermal stability of γS-crystallin as estimated by both tryptophan fluorescence and CD at 218 nm. When monitored by tryptophan fluorescence, the G18V mutation converts the transition curve into a three-state model, beginning just above 42 °C and continuing the transition until approximately 70 °C with two apparent steps. However, when monitored by CD at 218 nm, only a single transition is apparent, with a sharp transition at 65 °C, a decrease of 10 deg relative to the wild type. This suggests that the G18V mutation causes mild changes in the structure at temperatures between 42 and 60 °C, altering the microenvironment of the normally buried tryptophans although the basic protein fold remains intact. Then at 65 °C the amino and carboxy domains denature in quick succession as reflected by the sharp transition in the CD curve. Subsequently, the unfolded species were aggregation prone, consistent with the progressive cataract formation seen clinically (*15*).

Dynamic stabilities of the wild-type and mutant proteins were examined in greater detail by equilibrium unfolding/refolding in GuHCl. Wild-type HγS-crystallin demonstrates a two-state transition, suggesting that the two domains of γS-crystallins have similar stabilities, as has been previously described (*17*). The NMR solved structure of murine γS-crystallin also demonstrated high structural similarity among domains (*22*). Inefficiency in refolding γ-crystallins below 1 M GuHCl also has been noted previously (*19*). In contrast to wild-type HγS-crystallin the G18V mutant follows a biphasic transition, similar to the transitions seen with substitutions of alanine adjacent to the interface of γD-crystallin, R79A and M147A (*19*). While the alanine substitutions are proposed to destabilize the amino-terminal domain by increasing exposure of hydrophobic interface residues to solvent, the G18V mutation is predicted to destabilize the first Greek key motif directly (*2*). However, as with the R79A and M147A changes, the most likely explanation for our results is that the G18V substitution destabilizes the N-terminal domain selectively, so that a stable intermediate in the form of partially unfolded protein exists at intermediate levels of GuHCl. The second transition, presumably between the intermediate and unfolded state, occurs very close to that of the wild-type molecule, suggesting that stability of the C-terminal domain is minimally affected by the G18V mutation.

The free energies of partial unfolding, $\Delta G°$NI (2.58 kcal/mol for the mutant) are less than those required for unfolding to a totally denatured protein (4.83 kcal/mol), although the G18V mutant requires almost the same energy for the second step of unfolding as the wild type. There was a little difference in transition midpoints estimated here from previous studies, which can be interpreted with caution as stability measures are dependent upon the experimental conditions (pH, ionic strength, temperature, and protein concentration) which may differ between laboratories.

The G18V mutation occurring at the terminal end of the first strand in the first Greek motif of HγS-crystallin has been associated with autosomal dominant progressive cortical cataracts (*7*). The cortical location of this cataract is consistent with the known expression pattern of γS-crystallin, which tends to be most highly expressed in cortical fiber cells (*23*). CRYGS mutations have also been associated with a lamellar cataract (*24*), also consistent with the CRYGS expression pattern and a total cataract with denser opacity in the nucleus (*25*), suggesting the possibility of a more severe mutation. As discussed more fully elsewhere (*8*), mutations in crystallins that are sufficient in and of themselves to cause immediate protein aggregation or denaturation usually result in congenital cataract, while less severe mutations that merely increase susceptibility to environmental insults tend to contribute to age-related cataract. The results of these studies indicate normal association and structural properties of the G18V mutant γS-crystallin under mild conditions, but increased sensitivity stress, which are thus consistent with the progressive nature of the cataracts in this family. Mutations in several additional genes are associated with progressive cataract, including CRYGD, CRYBB2, GJA8, MIP, and BFSP2 (*26*−*30*). However, the molecular basis of most of these progressive cataracts is unclear. The molecular R14C mutation in γD-crystallin, which is also associated with progressive juvenile-onset hereditary cataracts, results in a mutant protein with nearly

identical secondary and tertiary structures and stabilities but appears to have increased susceptibility to oxidative formation of disulfide-mediated oligomers and subsequent aggregation (*31*).

Isolated cortical cataracts with Mendelian inheritance are relatively rare, but secondary and age-related cortical cataracts are common. Diabetes mellitus and hyperglycemia are major modifiable risk factors for the development of cortical cataract (*32*). The potential role of mutations in age-related cortical cataracts is emphasized by estimates from a twin study in the United Kingdom that two-thirds of age-related cortical cataracts can be explained by genetic factors (*33*). The Beaver Dam eye study has reported that a single major gene can account for 58% of the variability of age- and sex-adjusted measures of cortical cataract (*34*) and identified a major locus on chromosome 6p12-q12 (*35*).

Our present study further confirms the high stability of wild-type HγS-crystallin and demonstrates that the G18V mutation leads to destabilization of HγS-crystallin when subjected to heat and GuHCl-induced stress. These findings are consistent with the progressive nature of the cataracts in individuals carrying this mutation. In this family the lenses of affected individuals are initially clear or mildly opaque, but over time environmental stress results in progression to fully developed cortical cataracts (*7*). We are currently addressing the further pathogenesis of cataracts resulting from this mutation by studying the effects of G18V HγS-crystallin in the lenses of transgenic mice.

REFERENCES

1. Lubsen, N. H., Aarts, H. J. M., and Schoenmakers, J. G. G. (1988) The evolution of lenticular proteins: the beta- and gamma-crystallin supergene family. *Prog. Biophys. Mol. Biol. 51*, 47–76.
2. Blundell, T., Lindley, P., Miller, L., Moss, D., Slingsby, C., Tickle, I., Turnell, B., and Wistow, G. (1981) The molecular structure and stability of the eye lens: x-ray analysis of gamma-crystallin II. *Nature 289*, 771–777.
3. Shimeld, S. M., Purkiss, A. G., Dirks, R. P., Bateman, O. A., Slingsby, C., and Lubsen, N. H. (2005) Urochordate betagamma-crystallin and the evolutionary origin of the vertebrate eye lens. *Curr. Biol. 15*, 1684–1689.
4. Bloemendal, H., De, J. W., Jaenicke, R., Lubsen, N. H., Slingsby, C., and Tardieu, A. (2004) Ageing and vision: structure, stability and function of lens crystallins. *Prog. Biophys. Mol. Biol. 86*, 407–485.
5. Sinha, D., Esumi, N., Jaworski, C., Kozak, C. A., Pierce, E., and Wistow, G. (1998) Cloning and mapping the mouse Crygs gene and non-lens expression of gammaS-crystallin. *Mol. Vision 4*, 8.
6. Wang, X., Garcia, C. M., Shui, Y. B., and Beebe, D. C. (2004) Expression and regulation of alpha-, beta-, and gamma-crystallins in mammalian lens epithelial cells. *Invest. Ophthalmol. Visual Sci. 45*, 3608–3619.
7. Sun, H., Ma, Z., Li, Y., Liu, B., Li, Z., Ding, X., Gao, Y., Ma, W., Tang, X., Li, X., and Shen, Y. (2005) Gamma-S crystallin gene (CRYGS) mutation causes dominant progressive cortical cataract in humans. *J. Med. Genet. 42*, 706–710.
8. Shiels, A., and Hejtmancik, J. F. (2007) Genetic origins of cataract. *Arch. Ophthalmol. 125*, 165–173.
9. Cole, J. L., and Hansen, J. C. (2003) Analytical ultracentrifugation as a contemporary biomolecular research tool. *J. Biomol. Tech. 10*, 163–176.
10. Sreerama, N., and Woody, R. W. (2000) Estimation of protein secondary structure from circular dichroism spectra: comparison of CONTIN, SELCON, and CDSSTR methods with an expanded reference set. *Anal. Biochem. 287*, 252–260.
11. Sreerama, N., Venyaminov, S. Y., and Woody, R. W. (2000) Estimation of protein secondary structure from circular dichroism spectra: inclusion of denatured proteins with native proteins in the analysis. *Anal. Biochem. 287*, 243–251.
12. Pace, C. N., Shirley, B. A., and Thomson, J. (21990) Measuring the conformational stability of proteins, in Protein Structure: a Practical Approach (Creighton, T. E., Ed.) pp 311−330, IRL Press, Oxford.
13. Pace, C. N. (1986) Determination and analysis of urea and guanidine hydrochloride denaturation curves. *Methods Enzymol. 131*, 266–280.
14. Mills, I. A., Flaugh, S. L., Kosinski-Collins, M. S., and King, J. A. (2007) Folding and stability of the isolated Greek key domains of the long-lived human lens proteins {gamma}D-crystallin and {gamma}-S-crystallin. *Protein Sci. 16*, 2427–2444.
15. Kosinski-Collins, M. S., and King, J. (2003) In vitro unfolding, refolding, and polymerization of human gammaD crystallin, a protein involved in cataract formation. *Protein Sci. 12*, 480–490.
16. Hemmingsen, J. M., Gernert, K. M., Richardson, J. S., and Richardson, D. C. (1994) The tyrosine corner: a feature of most Greek key beta-barrel proteins. *Protein Sci. 3*, 1927–1937.
17. Wenk, M., Herbst, R., Hoeger, D., Kretschmar, M., Lubsen, N. H., and Jaenicke, R. (2000) Gamma S-crystallin of bovine and human eye lens: solution structure, stability and folding of the intact two-domain protein and its separate domains. *Biophys. Chem. 86*, 95–108.
18. Zarina, S., Slingsby, C., Jaenicke, R., Zaidi, Z. H., Driessen, H., and Srinivasan, N. (1994) Three-dimensional model and quaternary structure of the human eye lens protein gamma S-crystallin based on beta- and gamma-crystallin X-ray coordinates and ultracentrifugation. *Protein Sci. 3*, 1840–1846.
19. Flaugh, S. L., Kosinski-Collins, M. S., and King, J. (2005) Interdomain side-chain interactions in human gammaD crystallin influencing folding and stability. *Protein Sci. 14*, 2030–2043.
20. Wetzel, R. (1994) Mutations and off-pathway aggregation of proteins. *Trends Biotechnol. 12*, 193–198.
21. Tsonev, L. I., and Hirsh, A. G. (2000) Fluorescence ratio intrinsic basis states analysis: a novel approach to monitor and analyze protein unfolding by fluorescence. *J. Biochem. Biophys. Methods 45*, 1–21.
22. Wu, Z., Delaglio, F., Wyatt, K., Wistow, G., and Bax, A. (2005) Solution structure of (gamma)S-crystallin by molecular fragment replacement NMR. *Protein Sci. 14*, 3101–3114.
23. Ueda, Y., Duncan, M. K., and David, L. L. (2002) Lens proteomics: the accumulation of crystallin modifications in the mouse lens with age. *Invest. Ophthalmol. Visual Sci. 43*, 205–215.
24. Devi, R. R., Yao, W., Vijayalakshmi, P., Sergeev, Y. V., Sundaresan, P., and Hejtmancik, J. F. (2008) Crystallin gene mutations in Indian families with inherited pediatric cataract. *Mol. Vision 14*, 1157–1170.
25. Vanita, V., Singh, J. R., Singh, D., Varon, R., and Sperling, K. (2009) Novel mutation in the gamma-S crystallin gene causing autosomal dominant cataract. *Mol. Vision 15*, 476–481.
26. Stephan, D. A., Gillanders, E., Vanderveen, D., Freas-Lutz, D., Wistow, G., Baxevanis, A. D., Robbins, C. M., VanAuken, A., Quesenberry, M. I., Bailey-Wilson, J., Juo, S. H., Trent, J. M., Smith, L., and Brownstein, M. J. (1999) Progressive juvenile-onset punctate cataracts caused by mutation of the gammaD-crystallin gene. *Proc. Natl. Acad. Sci. U.S.A. 96*, 1008–1012.
27. Yao, K., Tang, X., Shentu, X., Wang, K., Rao, H., and Xia, K. (2005) Progressive polymorphic congenital cataract caused by a CRYBB2 mutation in a Chinese family. *Mol. Vision 11*, 758–763.
28. Willoughby, C. E., Arab, S., Gandhi, R., Zeinali, S., Arab, S., Luk, D., Billingsley, G., Munier, F. L., and Heon, E. (2003) A novel GJA8 mutation in an Iranian family with progressive autosomal dominant congenital nuclear cataract. *J. Med. Genet. 40*, e124.
29. Francis, P., Berry, V., Bhattacharya, S., and Moore, A. (2000) Congenital progressive polymorphic cataract caused by a mutation in the major intrinsic protein of the lens, MIP (AQP0). *Br. J. Ophthalmol. 84*, 1376–1379.
30. Conley, Y. P., Erturk, D., Keverline, A., Mah, T. S., Keravala, A., Barnes, L. R., Bruchis, A., Hess, J. F., FitzGerald, P. G., Weeks, D. E., Ferrell, R. E., and Gorin, M. B. (2000) A juvenile-onset, progressive cataract locus on chromosome 3q21-q22 is associated with a missense mutation in the beaded filament structural protein-2. *Am. J. Hum. Genet. 66*, 1426–1431.
31. Pande, A., Pande, J., Asherie, N., Lomakin, A., Ogun, O., King, J. A., Lubsen, N. H., Walton, D., and Benedek, G. B. (2000) Molecular basis of a progressive juvenile-onset hereditary cataract. *Proc. Natl. Acad. Sci. U.S.A. 97*, 1993–1998.
32. Hennis, A., Wu, S. Y., Nemesure, B., and Leske, M. C. (2004) Risk factors for incident cortical and posterior subcapsular lens opacities in the Barbados eye studies. *Arch. Ophthalmol. 122*, 525–530.
33. Hammond, C. J., Duncan, D. D., Snieder, H., de Lange, M., West, S. K., Spector, T. D., and Gilbert, C. E. (2001) The heritability of age-related cortical cataract: the twin eye study. *Invest. Ophthalmol. Visual Sci. 42*, 601–605.
34. Heiba, I. M., Elston, R. C., Klein, B. E., and Klein, R. (1995) Evidence for a major gene for cortical cataract. *Invest. Ophthalmol. Visual Sci. 36*, 227–235.
35. Iyengar, S. K., Klein, B. E., Klein, R., Jun, G., Schick, J. H., Millard, C., Liptak, R., Russo, K., Lee, K. E., and Elston, R. C. (2004) Identification of a major locus for age-related cortical cataract on chromosome 6p12-q12 in the Beaver Dam eye study. *Proc. Natl. Acad. Sci. U.S.A. 101*, 14485–14490.